HHS Public Access

Author manuscript

Brain Struct Funct. Author manuscript; available in PMC 2019 July 01.

Published in final edited form as:

Brain Struct Funct. 2018 July ; 223(6): 2609–2625. doi:10.1007/s00429-018-1649-6.

In vivo relationship between serotonin 1A receptor binding and gray matter volume in the healthy brain and in major depressive disorder

Francesca Zanderigo[1,2], **Spiro Pantazatos**[1,2], **Harry Rubin-Falcone**[1], **R. Todd Ogden**[1,2,3], **Binod Thapa Chhetry**[1], **Gregory Sullivan**[1], **Maria Oquendo**[1,2], **Jeffrey M. Miller**[1,2], and **J. John Mann**[1,2,4]

[1]Molecular Imaging and Neuropathology Division, New York State Psychiatric Institute, 1051 Riverside Drive, New York, NY 10032, USA

[2]Department of Psychiatry, Columbia University, 1051 Riverside Drive, New York, NY 10032, USA

[3]Department of Biostatistics, Columbia University, Mailman School of Public Health, 722 W 168th Street, New York, NY 10032, USA

[4]Department of Radiology, Columbia University, 622 W 168th Street, New York, NY 10032, USA

Abstract

Serotonin 1A (5-HT_{1A}) receptors mediate serotonin trophic role in brain neurogenesis. Gray matter volume (GMV) loss and 5-HT_{1A} receptor binding alterations have been identified in major depressive disorder (MDD). Here we investigated the relationship between 5-HT_{1A} receptor binding and GMV in 40 healthy controls (HCs) and, for the first time, 47 anti-depressant-free MDD patients using Voxel-Based Morphometry and [^{11}C]WAY100635 Positron Emission Tomography. Values of GMV and 5-HT_{1A} binding (expressed as BP_F, one of the types of binding potentials that refer to displaceable or specific binding that can be quantified in vivo with PET) were obtained in 13 regions of interest, including raphe, and at the voxel level. We used regression analysis within each group to predict GMV from BP_F, while covarying for age, sex, total gray matter volume and medication status. In the HCs group, we found overall a positive correlation between terminal field 5-HT_{1A} receptor binding and GMV, which reached statistical significance in regions such as hippocampus, insula, orbital prefrontal cortex, and parietal lobe. We observed a trend towards inverse correlation between raphe 5-HT_{1A} autoreceptor binding and anterior cingulate GMV in both groups, and a statistically significant positive correlation between raphe 5-HT_{1A} binding and temporal GMV in MDD. Analysis of covariance at the voxel-level revealed a trend towards interaction between diagnosis and raphe 5-HT_{1A} binding in predicting GMV in cerebellum and supramarginal gyrus (higher correlation in HCs compared with MDD). Our results replicated previous findings in the normative brain, but did not extend them to the brain in MDD,

Correspondence to: Francesca Zanderigo.

Conflict of interest Drs. Zanderigo and Ogden, Mr. Rubin-Falcone and Mr. Binod Thapa Chhetry have no conflicts of interest to declare. Dr. Pantazatos's contribution to this work was supported by NIMH K01MH108721. Drs. Mann and Oquendo receive royalties for commercial use of the Columbia-Suicide Severity Rating Scales from the Research Foundation for Mental Hygeine and Dr. Oquendo receives an honorarium as President of the American Psychiatric Association. Her family owns stock in Bristol Myers Squibb. Dr. Miller's family previously owned stock in Johnson & Johnson, unrelated to the current manuscript. Dr. Sullivan is currently employed by Tonix Pharmaceuticals, Inc. and holds stock in the same, unrelated to the current manuscript.

and indicated a trend towards dissociation between MDD and HCs in the relationship of raphe 5-HT_{1A} binding with postsynaptic GMV. These results suggest that 5-HT_{1A} receptors contribute to altered neuroplasticity in MDD, possibly via effects predating depression onset.

Keywords

Positron emission tomography; Magnetic resonance imaging; Serotonin 1A receptor; Gray matter volume; Major depressive disorder

Introduction

Serotonin (5-HT) plays a role in brain development, neurogenesis, neuronal morphology and circuit formation (Daubert and Condron 2010; Dayer 2014; Gaspar et al. 2003). In particular, 5-HT_{1A} receptors are involved in actions that provide intracellular stability for the cytoskeleton and result in cell differentiation and cessation of proliferation (Azmitia 2001). Neurobiological studies have identified second messenger pathways that exert neuroplastic changes (Citri and Malenka 2008; Pittenger and Duman 2008) triggered by 5-HT via 5-HT_{1A} receptors (Azmitia 2001; Tardito et al. 2006). Brain heteroreceptor complexes of fibroblast growth factor receptor 1 (FGFR1) and 5-HT_{1A} receptors are described in the rat in both hippocampus and in midbrain 5-HT neurons, and agonist coactivation in these complexes enhances FGFR1 signaling leading to increased neuroplasticity and antidepressant-like actions (Borroto-Escuela et al. 2015a, b, 2016).

Dysfunctional neuronal organization is thought to contribute to the pathogenesis of major depressive disorder (MDD) and other psychiatric disorders (Pittenger and Duman 2008; van Spronsen and Hoogenraad 2010). Studies using structural magnetic resonance imaging (MRI) have identified gray matter volume (GMV) loss in MDD (Dep-ping et al. 2015; Goodkind et al. 2015), most commonly in the hippocampal formation (Benninghoff et al. 2010; Geuze et al. 2005; Malykhin and Coupland 2015). Conversely, MRI studies have also reported increased GMV in response to trophic effects of motoric training, cognitive performance or treatment with selective serotonin reuptake inhibitors (Draganski et al. 2004; Kanai and Rees 2011; Maya Vetencourt et al. 2008; Smith et al. 2013). However, the underlying molecular mechanisms leading to gray matter loss or gain in these disorders are not well-understood. Positron emission tomography (PET) studies have also demonstrated differences in 5-HT_{1A} receptor density in MDD (Drevets et al. 2007; Miller et al. 2009; Parsey et al. 2010, 2006b; Savitz et al. 2009; Savitz and Drevets 2009), particularly in the raphe (Salvadore et al. 2011; Savitz et al. 2009; van Tol et al. 2010). We found elevated 5-HT_{1A} binding across many brain regions including the raphe in current MDD in studies of three independent cohorts using the 5-HT_{1A} receptor antagonist radiotracer [^{11}C]WAY100635 (Miller et al. 2013; Parsey et al. 2006b, 2010), while other PET studies have reported divergent findings in MDD (Drevets et al. 1999, 2007; Melt-zer et al. 2004; Sargent et al. 2000). We found that these discrepancies are explained by differences in imaging data analytic methods when applied to the same sample (Parsey et al. 2010) (please refer to (Parsey et al. 2010) for a discussion of the topic).

5-HT_{1A} receptors might be involved in altering GMV by mediating neurotrophic effects, thereby offering a possible explanation for gray matter alterations observed in MDD. Kraus et al. (Kraus et al. 2012) imaged 35 healthy subjects with both PET and MRI and found a positive correlation between postsynaptic 5-HT_{1A} receptor binding and GMV in several regions including hippocampus and temporal cortex, and between presynaptic 5-HT_{1A} receptor binding in the raphe and GMV in forebrain projection sites. However, this relationship has not been studied in MDD.

Here we investigated the relationship between in vivo 5-HT_{1A} receptor binding and GMV in healthy controls (HCs) and in antidepressant-free depressed patients with MDD, using voxel-based morphometry (VBM) (Wright et al. 1995) and PET with [^{11}C]WAY100635 (Parsey et al. 2000; Pike et al. 1996), and distinguishing between 5-HT_{1A} raphe autoreceptors and terminal field 5-HT_{1A} receptors. The in vivo 5-HT_{1A} receptor binding was expressed using the binding potential BP_F (Innis et al. 2007), which measures displaceable specific binding ($BP_F = B_{avail}/K_D$, where K_D is the tracer equilibrium dissociation constant and Bavail the density of available receptors) (Innis et al. 2007). We hypothesized that, in both groups, GMV in the terminal fields would be positively correlated with postsynaptic 5-HT_{1A} receptor binding, because 5-HT_{1A} receptors mediate the 5-HT trophic effect in brain (Persico et al. 2006). We also hypothesized that 5-HT_{1A} autoreceptor binding would be inversely correlated with GMV, because 5-HT_{1A} autoreceptors in the raphe nuclei inhibit firing and serotonin release.

Materials and methods

Subjects

Forty HCs (19 females; 21 males), aged 18–69 years, and forty-seven individuals with MDD (30 females; 17 males), aged 20–70 years, who were recruited during previously published studies (Parsey et al. 2006b, 2010; Sullivan et al. 2015), were included in this analysis. Eligibility assessment included medical and psychiatric history, physical examination, routine blood tests, urinalysis, urine toxicology, and electrocardiogram.

HCs were able to provide informed consent, had no history of an Axis I or Axis II psychiatric disorder (including absence of current or past alcohol or substance abuse or dependence), no family history of a mood disorder or schizophrenia, no significant medical illness, and they were free of antidepressant and all medications that may affect specifically the serotonin system. For the HCs, the Structured Clinical Interview for DSM-IV Axis I Disorders (non-patient version-SCID NP) (First et al. 2012) was used to evaluate study eligibility. Exclusion criteria included: (1) past or present substance or alcohol abuse or dependence; (2) history of IV drug use; (3) 3,4-methylenedioxy-methamphetamine (MDMA; ecstasy) use more than three times; (4) lack of capacity to provide informed consent; (5) if female, pregnancy or plans to conceive during the course of study participation; (6) current, past or anticipated exposure to radiation in the workplace, or participation in nuclear medicine procedures, including research protocols; (7) heart pacemaker, body implant or other metal in body; (8) lactation.

For the individuals with MDD, psychiatric diagnoses were established using the Structured Clinical Interview for DSM-IV (First et al. 1995), conducted by doctoral- or master-level psychologists and reviewed in a consensus conference of research psychologists and psychiatrists. Depression severity was quantified with the Hamilton Rating Scale for Depression (HRSD) (Hamilton 1960) and the Beck Depression Inventory (BDI) (Beck et al. 1961). Inclusion criteria for the MDD sample included: (1) MDD in a current major depressive episode as defined by means of the SCID; (2) 17-item HRSD ≥ 16; (3) age 18–75; (4) off of all psychotropic medications likely to interact with 5-HT_{1A} receptors for a minimum of 14 days at the time of scan; (5) off of neuroleptics for a minimum of 1 month and fluoxetine for a minimum of 6 weeks prior to time of scan; (6) off of serotonin depleting drugs such as reserpine for a minimum of 3 months at the time of scan. Short acting benzodiazepines were allowed for distressing anxiety or insomnia up to 24 h prior to PET scan. Exclusion criteria included: (1) other major psychiatric disorders such as lifetime schizophrenia, schizoaffective illness, bipolar disorder or current drug or alcohol abuse (within 2 months for abuse or 6 months for dependence); anorexia nervosa or bulimia nervosa in the past year; (2) family history of schizophrenia; (3) significant active physical illness, particularly those that may affect the brain or serotonergic system, including blood dyscrasias lymphomas, hypersplenism, endocrinopathies, renal failure or severe chronic obstructive lung disease, autonomic neuropathies and active malignancy; (4) incapacity to consent; (5) being actively suicidal; (6) electroconvulsive therapy (ECT) within the last 3 months for current episode; (7) history of non-response to ECT in the last 2 years; (8) if female, pregnancy or plans to conceive during the course of study participation; (9) current, past or anticipated exposure to radiation in the workplace, or participation in nuclear medicine procedures, including research protocols; (10) heart pacemaker, body implant or other metal in body; (11) lactation.

We did not explicitly match our sample for age or sex between patients and MDD participants, and they did not differ significantly between groups (Table 1). We did consider them as covariates in our analyses, since they had an effect on the outcome variable. Additional subject information, including ethnicity, educational attainment, depression severity, psychiatric comorbidity, and, among depressed participants, number of previous depressive episodes as well as length of the current major depressive episode, are included in Table 1.

The Institutional Review Board of the New York State Psychiatric Institute approved the protocol, and all subjects provided informed consent after an explanation of the study protocol and associated risks.

MRI images

Acquisition

All subjects underwent a three-dimensional spoiled gradient recalled acquisition (3D-SPGR) T1-weighted axial MRI scan, acquired with a 1.5-T GE Signa Advantage scanner (General Electric Medical Systems, Milwaukee, Wisconsin) at a resolution of 1.5 × 0.9 × 1.0 mm. The sequence parameters were: TR 34 ms, TE 5 ms, flip angle 45°, slice thickness 1.5 mm, 124 slices, FOV 22 × 16 cm^2, 256 × 193 matrix reformatted to 256 × 256 with 1.5 × 0.78 × 0.78

mm^3 voxels. Detailed quality control using visual inspection was carried out to rule out any motion artifacts and gross neuropathology.

Image processing

The T1-weighted images were processed with Statistical Parametric Mapping 8 (SPM8) software package (http://www.fil.ion.ucl.ac.uk/spm; Wellcome Department of Imaging Neuroscience) using VBM8 toolbox (http://dbm.neuro.uni-jena.de/vbm/). Images were bias corrected, segmented, and spatially normalized to standard Montreal Neurological Institute (MNI) space at a voxel size of 1.5 × 1.5 × 1.5 mm^3 using 12-parameter affine linear transformation and diffeomorphic anatomical registration through exponentiated lie algebra (DARTEL) (Ashburner 2007). To preserve the actual gray matter values locally, segmented gray matter images were multiplied by the measure of warped and unwarped structures derived from the nonlinear step of the spatial normalization. The modulated gray matter volume (referred to as GMV) images were smoothed with an iso-tropic Gaussian kernel of 8 mm full width at half maximum (FWHM). Regions of interest (ROI) GMV values were taken as the average GMV values within standard space versions of the ROI masks used for PET analysis, as described below.

PET images

Radiochemistry and input function measurement

All subjects were scanned with [^{11}C]WAY100635. For details of radiotracer preparation, see Parsey et al. (Parsey et al. 2006b). A metabolite-corrected arterial input function was obtained in each subject (Parsey et al. 2000). Plasma free fraction (f_P) of [^{11}C]WAY100635 was assayed in triplicate (Parsey et al. 2006b).

Image acquisition and analysis

PET images were acquired from an ECAT EXACT HR + scanner (Siemens/CTI, Knoxville, Tennessee) as previously described (Parsey et al. 2000). The PET camera generated 47 slices covering an axial field of view of 16.2 cm, with transverse and axial resolutions at the center of the field of view that were 6.0 and 4.6 mm FWHM, respectively, in 3D mode. The axial sampling was 3.4 mm. A 15-min transmission scan was obtained, followed by a bolus injection of [^{11}C]WAY100635 (over 30 s) and by an emission scan of 110 min of 20 frames of increasing duration (3 × 20 s, 3 × 1 min, 3 × 2 min, 2 × 5 min, 9 × 10 min). Images were reconstructed to a 128 × 128 matrix (pixel size of 2.5 × 2.5 mm^2). To correct for residual subject motion during PET scanning, PET frames were registered to the eighth frame using the FMRIB linear image registration tool (FLIRT), version 5.0 (FMRIB Image Analysis Group, Oxford, UK). Each participant's mean PET image was co-registered to the corresponding MRI using FLIRT with a mutual information cost function, six degrees of freedom, and trilinear interpolation, optimized as previously described (Milak et al. 2010). Detailed quality control using visual inspection was carried out on the final corrected images. We reviewed and approved each step of pre-processing, including motion correction, by watching a movie of uncorrected and corrected 4D volumes, in axial, sagittal, and coronal orientations. Twelve anatomical ROIs that our group had considered in several previous publications with the tracer [^{11}C]WAY100635 (Parsey et al. 2000, 2006a, b, 2010),

which encompass a broad anatomic array of cortical and subcortical structures with appreciable 5-HT_{1A} binding, were traced on individuals' T1-weighted MRIs based on brain atlases (Duvernoy 1991; Talairach and Tournoux 1988) and published reports (Parsey et al. 2010). ROIs consisted of anterior cingulate, amygdala, cingulate, dorsolateral prefrontal cortex, hippocampus, insula, medial prefrontal cortex, occipital lobe, orbital prefrontal cortex, parietal lobe, parahippocampal gyrus, and temporal lobe. To label the raphe nuclei, a fixed volume elliptical ROI (2 cm^3) was placed in the dorsal midbrain: such volume is a composite of mostly the dorsal and median raphe nuclei, and was obtained using a mean PET image for each subject, since the boundaries of this structure cannot be identified on MRI. A cylindrical ROI was delineated manually in the cerebellar white matter as a reference region. The size and exact location of such region varied subject-by-subject, but the method used for delineation has previously been shown to produce a reliable reference region (Parsey et al. 2005). Each subject's mean PET image was co-registered to their MRI using FLIRT, as previously described (DeLorenzo 2009). ROI-level time activity curves were generated as the average activity measured across the voxels within each ROI over the time course of the PET acquisition. Both ROI- and voxel-level time activity curves were corrected for vascular contribution using a fixed fractional blood volume (V_B) of 5% before estimation of the PET outcome measure.

PET outcome measure estimation

ROI-level

Distribution volumes (V_T) of [^{11}C]WAY100635 were estimated for each ROI using kinetic analysis with a metabolite-corrected arterial input function and a two tissue compartment constrained (2TCC) model, in which the K_1/k_2 ratio in each ROI was constrained to that of the reference region (for more details, see Parsey et al. (Parsey et al. 2000)). The binding potential BP_F was then calculated in each ROI as $(V_T - V_{ND})/f_P$, where V_{ND} is the tracer non-displaceable distribution volume, estimated using the V_T in the reference region, the cerebellar white matter (Innis et al. 2007).

Voxel-level

BP_F was estimated at the voxel-level using a data-driven basis pursuit strategy (Gunn et al. 2002). Briefly, this approach is based on the compartmental theory commonly used for description of a PET radiotracer's kinetics, and determines a parsimonious model consistent with the measured data. The approach requires choosing a family of basis functions that is in a range physiologically plausible for the considered radiotracer. Here we used a range spaced in a logarithmic manner that was suggested for [^{11}C]WAY100635 to achieve a suitable coverage of the radiotracer kinetic spectrum (Gunn et al. 2002). Once the V_T parametric images were obtained in each subject, corresponding BP_F images were generated by subtracting in each voxel the average (across voxels within the ROI) V_T of the cerebellar white matter, and dividing for the subject measured f_P. BP_F images were transformed into subject-MRI space using the transformations obtained during coregistration, then normalized and resampled to MNI standard space with a voxel size of 1.5 × 1.5 × 1.5 mm^3 using the transformations obtained in the GMV processing of MRI images, spatially smoothed with an isotropic Gaussian kernel of 4 mm FWHM, and mean centered.

Statistical analysis

At the ROI-level, we fitted linear mixed effects models to the postsynaptic GMV values, using region, diagnostic group, and 5-HT_{1A} BP_F as fixed effects and subject as the random effect, to properly account for the covariance structure of the data and to allow for testing of a single effect that is consistent across ROIs. We repeated the analysis with only raphe 5-HT_{1A} autoreceptor BP_F (rather than ROI-specific estimates of binding) as a fixed effect. We also determined whether the effect of autoreceptor binding is consistent across all ROIs by testing for an interaction term. In each case, we also performed a post hoc analysis by exploring the individual ROI-specific effects. Specifically, this was done by examining the significance of the ROI-specific parameters within the linear mixed effects model (rather than performing modeling separately on the data from each ROI). All analyses were performed using R 3.3.0 (http://cran.r-project.org).

At the voxel-level, we performed the following analyses using Matlab 2012b (http://www.mathworks.com/) and the Wake Forest University SPM5 Biological Parametric Mapping toolbox (BPM beta version 1.5d) (Casanova et al. 2007).

1. Within each clinical group, we performed a multiple regression analysis to predict GMV (in each voxel) from 5-HT_{1A} receptor BP_F (in each voxel), while covarying for age, sex, total gray matter volume (TGMV; calculated during VBM normalization), and medication status. Medication status was defined as a binary variable: subjects were labeled as antidepressant naïve vs. antidepressant exposed, as our group has done in previous analyses (Parsey et al. 2010). More specifically, we defined subjects as antidepressant exposed to be those MDD subjects that had been on an adequate dose of anti-depressant for at least 4 weeks within the past 4 years, and as antidepressant naïve (or not recently medicated) those MDD individuals that had never been exposed to antidepressant medications, had a past trial of < 4 weeks, or had been off medications for more than 4 years (Parsey et al. 2010). HC subjects were considered as antidepressant naïve. A gray matter binary mask was applied to restrict the analysis to gray matter areas (> 0.5 probability). Areas of correlation were considered statistically significant at voxel-level corrected $p < 0.05$, $k > 50$, corrected for multiple comparisons using false discovery rate (FDR). An exploratory threshold of $p < 0.001$, uncorrected, $k > 10$ was also applied when no results survived the above threshold. This threshold was used as a cluster-forming threshold to apply cluster-extent thresholding as implemented through AFNI's 3DClust-Sim (v. May 19, 2015). At this uncorrected threshold, clusters larger than 215 voxels were deemed significant at $p < 0.05$ corrected. Given that voxel-wise thresholding may be overly stringent when correcting for thousands of comparisons across the brain, we also applied uncorrected voxel-wise ($p < 0.001$, $k > 10$) and cluster-extent corrected thresholding (clusters formed using an uncorrected $p < 0.001$) given its higher sensitivity to weaker, yet spatially distributed, effects.
2. We performed an analysis of covariance (ANCOVA), with independent factors of diagnosis (HC vs. MDD) and 5-HT_{1A} receptor BP_F, to identify areas of the brain

where the correlation between BP_F and GMV (in each voxel, adjusted for age, gender, TGMV, and medication status) differed between HC and MDD group. Similarly to the analysis above, uncorrected ($p < 0.001$, $k > 10$) at voxel-level and cluster-extent thresholding ($p < 0.05$ corrected, see above) were applied.

Analyses (1) and (2) above were repeated to predict GMV (in each voxel) from raphe 5-HT_{1A} autoreceptor BP_F (from the quantification at the ROI-level) while covarying for age, sex, TGMV, and medication status. Note that in this case the voxel-wise analyses did not use the BPM toolbox but rather used a standard SPM8 analysis.

For the voxel-level analysis, regions were labeled using the Wake Forest University (WFU) Pickatlas toolbox (Maldjian et al. 2003).

In all analyses, BP_F data were first log transformed to remedy slight skewness of binding estimates (Hirvonen et al. 2008; Meltzer et al. 2004; Rabiner et al. 2002).

Results

Sample

The study sample comprised 40 HCs (19 females; 21 males) and 47 MDD patients (30 females; 17 males), as described in Table 1. Depressed and control groups were comparable in terms of age, race and proportion of males and females. The MDD group had almost 2 years fewer of lifetime education. Years of education were not associated to ROI-level GMV values among the HCs, and they were positively associated to ROI-level GMV values only in the temporal lobe among the MDD patients (Pearson's $r = 0.358$, $p = 0.016$, uncorrected for multiple comparison). Weight, body surface, injected tracer dose and day of the year of PET scan were also comparable. The MDD group was injected a significantly higher specific activity and a significantly lower mass. Specific activity and injected mass, however, were not associated to ROI-level GMV values in either group. The MDD group was scanned significantly later in the day than the HC group (average time of scan for HCs was about 13.3 h past midnight, while average time for MDD was about 14.3 h past midnight). However, the average difference in scan times was an hour, which we do not expect to have reasonably affected binding across subjects and groups.

Covariates

In the ROI-level analyses reported below, we included three covariates in each model: age ($F = 31.85$; $df = 1, 80$; $p < 0.0001$), sex ($F = 19.07$; $df = 1, 80$; $p < 0.0001$), and TGMV ($F = 15.47$; $df = 1, 80$; $p = 0.0002$). We also included medication status as a covariate in the models involving depressed subjects.

Relationship between GMV and terminal field 5-HT_{1A} receptors BP_F

ROI-level

In the HC group, there was an overall positive association between 5-HT_{1A} BP_F and GMV ($F = 9.652$; $df = 1, 428$; $p = 0.0020$). The association seemed to be fairly consistent across all considered ROIs (test for region × binding interaction: $F = 1.320$; $df = 11, 417$; $p = 0.210$).

Post hoc testing for ROIs that showed a significant relationship between 5-HT_{1A} BP_F and GMV were: amygdala, hippocampus, insula, occipital lobe, orbital prefrontal cortex, parietal lobe, with trend-level relationships in dorsolateral prefrontal cortex and temporal lobe. The estimated relationship was positive for all regions, with the exception of anterior cingulate bilaterally.

In the MDD group, the overall effect of 5-HT_{1A} BP_F on GMV was not significant (F = 2.267; df = 1, 505; p = 0.133). Within the linear mixed model for MDD subjects, the only ROI that showed a significant relationship was the temporal lobe; the parahippocampal gyrus had a trend-level effect. In each of these regions, we observed a positive relationship between 5-HT_{1A} BP_F and GMV.

In a model including both diagnostic groups, we observed no statistically significant interaction between diagnosis and BP_F in predicting GMV.

Voxel-level

In the HC group, statistically significant positive correlations were observed in supramarginal gyrus, temporal gyrus, hippocampus, parahippocampal gyrus, precentral gyrus, and dorsolateral prefrontal cortex (Fig. 1; Table 2, $p < 0.05$ FDR-corrected, $k > 50$). No clusters showed a negative correlation at this threshold.

In the MDD group, statistically significant positive correlations were observed in parietal cortex, inferior temporal gyrus, temporal pole, occipital/fusiform gyrus, supra-marginal gyrus, and dorsolateral prefrontal cortex (Fig. 1; Table 3, $p < 0.05$ FDR-corrected, $k > 50$). At this threshold, only one cluster (in the cerebellum) showed a negative correlation (Fig. 1, top row).

ANCOVA did not reveal significant interaction effects between diagnosis and 5-HT_{1A} BP_F in predicting GMV at the applied voxel-wise ($p < 0.05$ FDR-corrected, $k > 50$) and cluster-extent corrected threshold ($p < 0.05$). At an exploratory threshold, the most pronounced interaction was greater BP_F-GMV association in MDD (vs. HC) in the precentral gyrus ($p <$ 0.001 uncorrected, cluster size = 146, Table 4).

Relationship between GMV and raphe 5-HT_{1A} autoreceptor BP_F

ROI-level

In the HC group, there was no significant association between raphe 5-HT_{1A} autoreceptor BP_F and cortical GMV considering all regions together (F = 0.026; df = 1, 35; p = 0.872), nor was there evidence of a region × binding interaction. Allowing for a different relationship within each region in the framework of the mixed effects model, the only significant region was the anterior cingulate, which showed a negative relationship.

In the MDD group, we did not find an overall (consistent across regions) effect of raphe binding (F = 0.004; df = 1, 41; p = 0.952), although there was a significant interaction between region and raphe binding (F = 2.252; df = 1, 495; p = 0.011). Post hoc testing showed a significant positive relationship between raphe 5-HT_{1A} autoreceptor BP_F and

cortical GMV in the temporal lobe, and a significant negative relationship in the anterior cingulate.

We also analyzed data from all the subjects together in a single model to examine the potential effect of diagnostic group (defined for this analysis to include three groups: controls, MDD med-exposed, and MDD med-naïve) on GMV, also including autoreceptor binding and the other covariates. We found no main effect of group ($F = 2.75$; $df = 2, 8$; $p = 0.070$), and we also saw no evidence of an interaction between group and raphe 5-HT_{1A} autoreceptor BP_F ($F = 0.26$; $df = 2, 78$; $p = 0.769$).

Voxel-level

In the HC group, no voxels survived voxel-wise correction at $p < 0.05$ FDR. At an uncorrected threshold coupled with cluster-extent correction ($p < 0.05$ corrected), higher raphe 5-HT_{1A} autoreceptor BP_F predicted lower GMV in subgenual cingulate and posterior cingulate, and higher GMV in cerebellum (Fig. 2, Table 5).

In the MDD group, no voxels survived voxel-wise correction at $p < 0.05$ FDR. At an uncorrected threshold coupled with cluster-extent correction ($p < 0.05$ corrected), higher raphe 5-HT_{1A} autoreceptor BP_F predicted lower GMV in dorsolateral prefrontal cortex and lateral occipital cortex (Fig. 2, Table 5).

Voxel-level ANCOVA was used to determine whether correlations between raphe 5-HT_{1A} BP_F and cortical GMV were moderated by diagnosis. No voxels survived voxel-wise correction at $p < 0.05$ FDR. Using cluster-extent correction, we found higher association in HC vs. MDD in the cerebellum and supramarginal gyrus ($p < 0.05$ corrected) (Fig. 3, Table 5).

Discussion

We investigated the relationship between in vivo 5-HT_{1A} receptor binding and GMV in a group of HCs and, for the first time, in a group of antidepressant-free patients with MDD. We found that there is overall a positive association between terminal fields 5-HT_{1A} receptor binding and GMV in the HC group, but we found no evidence of such association in the MDD group, although there was a possible effect in the temporal lobe and the parahippocampal gyrus. We observed no significant association between raphe 5-HT_{1A} autoreceptors binding and other regions GMV in both groups, although an inverse relationship appeared at trend-level in the anterior cingulate in both groups, and a positive relationship appeared at trend-level in the temporal lobe in the MDD group.

Postsynaptic 5-HT_{1A} receptors binding and GMV in the terminal fields

Our results using the PET outcome measure BP_F are in agreement with previous findings in HCs that used the outcome measure BP_{ND} (Kraus et al. 2012), namely that there is overall a positive correlation between terminal fields 5-HT_{1A} receptor binding and GMV in HCs, which reaches statistical significance in a subset of regions such as hippocampus, insula, orbital prefrontal cortex and parietal lobe at the ROI-level, and in the hippocampus,

supramarginal, temporal, parahippocampal and precentral gyrus, and dorsolateral prefrontal cortex at the voxel-level. Interestingly, hippocampal GMV was previously associated with another serotonergic measure, 5-HT transporter gene methylation status, in humans (Dannlowski et al. 2014). Furthermore, brain fibroblast growth factor receptor 1 (FGFR1)-5-HT_{1A} heteroreceptor complexes, and their enhancement of neuro-plasticity, were first described in the hippocampus (Borroto-Escuela et al. 2016), where 5-HT_{1A} receptors may promote greater GMV, potentially protecting HCs against depression (Schmidt and Duman 2007). 5-HT_{1A} receptors in the hippocampus have been demonstrated to mediate neurogenesis and dendritic maturation (Yan et al. 1997).

We did not observe the same overall positive correlation between terminal fields 5-HT_{1A} receptor binding and GMV in the MDD group, with the possible exception of the temporal lobe and the parahippocampal gyrus (at trend-level) at the ROI-level, and the parietal cortex, inferior temporal, occipital/fusiform and supramarginal gyrus, temporal pole, and dorsolateral prefrontal cortex at the voxel-level.

There was no differential effect of postsynaptic 5-HT_{1A} receptor binding on GMV as a function of diagnosis in the terminal field ROIs, nor did we observe such an effect in voxel analyses at our a priori statistical threshold. Using an exploratory, less stringent threshold, the most pronounced interaction was observed at the voxel-level in the precentral gyrus, where the 5-HT_{1A} receptor BP_F-GMV association was greater in MDD (vs. HC). If confirmed in subsequent studies, this may suggest an uncoupling of 5-HT_{1A} receptor from trophic effects in depressed patients, which could be due to downstream signaling that is affected/uncoupled, to 5-HT_{1A} binding or GMV being driven by another factor, or to ceiling effects.

In the HC group, our results are consistent with our hypothesis that GMV in the terminal fields is positively correlated with postsynaptic 5-HT_{1A} receptor binding. As 5-HT_{1A} receptors contribute with other receptors to mediate the 5-HT trophic effect in the brain (Persico et al. 2006), a higher concentration of 5-HT_{1A} heteroreceptors postsynaptically would translate into an increased ability to transduce unit signal of 5-HT in the synapse. While the current study design cannot address causality, our findings provide support for a model of neuroplastic actions of 5-HT_{1A} receptors impacting regional amounts of gray matter, and justify additional research into this relationship. We found no confirmation of this hypothesis in the MDD group.

Raphe 5-HT_{1A} autoreceptors binding and GMV in the terminal fields

Overall, we found no significant association between raphe 5-HT_{1A} autoreceptor binding and other regional GMV in either one of the groups. However, we found a trend toward an inverse relationship in both the HC and MDD group between 5-HT_{1A} autoreceptor binding in raphe nuclei and anterior cingulate GMV. At the voxel-level, an inverse relationship between raphe 5-HT_{1A} autoreceptor binding and postsynaptic GMV was found in subgenual cingulate and posterior cingulate in the HC group, and in dorsolateral prefrontal cortex and lateral occipital cortex in the MDD group, only when using an uncorrected threshold coupled with cluster-extent correction. We hypothesized that there is a more widespread

inverse relationship between 5-HT_{1A} autoreceptor binding and terminal field GMV. The fact that regionally specific effects of raphe 5-HT_{1A} autoreceptor binding on anterior cingulate GMV were observed may be driven by the topography of the dorsal raphe nuclei (Jasinska et al. 2012a, b), suggesting the possibility that subnuclei that project to cingulate cortex may be driving this effect. The effect of 5-HT is trophic and 5-HT_{1A} autoreceptors regulate firing rate and 5-HT release throughout the brain (Nautiyal and Hen 2017). Mouse studies suggest that terminal field postsynaptic 5-HT_{1A} receptors are also needed for 5-HT-mediated neurogenesis (Nautiyal and Hen 2017). These studies support the idea that postsynaptic receptor function, or their relevant coupled second messenger systems, will also moderate 5-HT trophic effects and could vary between brain regions. Thus, while 5-HT_{1A} autoreceptors may relate to trophic effects, such effects may be differentially modulated in different terminal field brain regions by postsynaptic receptor signal transduction. We have previously reported a blunting of postsynaptic 5-HT_{1A}-mediated signal transduction in human brain postmortem in depressed suicides (Hsiung et al. 2003) that may explain the absence of such a correlation with gray matter in the MDD group.

Our hypothesis and our findings of an inverse correlation between presynaptic 5-HT_{1A} receptor binding and postsynaptic GMV are in contradiction with the positive correlation between raphe 5-HT_{1A} autoreceptor binding and GMV in the anterior cingulate cortex reported by Kraus et al. (Kraus et al. 2012). Kraus et al. hypothesized a correlation, but not the direction of the correlation, between raphe 5-HT_{1A} binding and GMV postsynaptically, and added GMV of the raphe in the regression model to eliminate potential confounding effects of raphe gray matter and whole brain gray matter interactions (Kraus et al. 2012), which was not part of our primary analytic approach. However, repeating our ROI-level analysis adding the covariate suggested by Kraus et al. did not change our findings of a negative correlation between raphe 5-HT_{1A} autoreceptor binding and anterior cingulate GMV. This discrepancy could be explained by the different PET outcome measures considered (BP_{ND} vs. BP_F), or by a different approach in the extraction of the PET signal in the raphe, which is notoriously hard to delineate from MRI images.

Differently from the HC group, in the MDD group, we found a statistically significant positive correlation between raphe 5-HT_{1A} autoreceptor binding and temporal lobe GMV, which was, however, not present at the voxel-level, at both corrected and uncorrected thresholds. An effect of interaction between diagnosis and raphe 5-HT_{1A} autoreceptors binding in predicting GMV was observed at the voxel-level only at the exploratory threshold in the cerebellum and supramarginal gyrus, where we found higher association in HC vs. MDD.

Overall, these results suggest that the 5-HT_{1A} receptor could be an interesting target in clinical studies on altered neuroplasticity in brain disorders, and suggest a possible neurodevelopmental pathway through which 5-HT_{1A} receptor levels may contribute to neurodevelopment in brain regions relevant to mood (Savitz et al. 2009), anxiety (Akimova et al. 2009) or cognition (Ogren et al. 2008).

ROI-versus voxel-level analysis

ROI- and voxel-level analyses present distinct advantages and disadvantages: the ROI-level approach reduces the number of multiple comparisons and increases power at the expense of reduced anatomical detail, while the voxel-level analyses provide increased anatomical detail at the expense of reduced sensitivity due to having to adjust for multiple comparisons. Although one does not necessarily expect entirely concordant results between the two analyses, we did observe some overlap in the results obtained at the ROI- and voxel-level. Specifically:

1. Postsynaptic 5-HT_{1A} receptors binding and GMV in the terminal fields: in both analyses, we observed a direct association in the HCs group in the hippocampus and dorsolateral prefrontal cortex, and a direct association in the MDD group in the temporal lobe; results from the interaction analysis were not significant at both the ROI-level and voxel–level, at the applied voxel-wise threshold correction.
2. Raphe 5-HT_{1A} autoreceptors binding and GMV in the terminal fields: although at trend-level, both analyses revealed an inverse correlation in the cingulate in the HCs group, and no significant correlation in the MDD group or in the interaction analysis.

Limitations

This is a retrospective, cross-sectional study that can only reveal correlation, but not causality, between PET- and MRI-based outcome measures; to investigate causality, an interventional study would be required.

At the level of resolution currently achieved by MRI scans used in clinical studies, there are ten thousands of interconnected neuronal and glial cells present in one single imaging voxel (Tost et al. 2010; Zatorre et al. 2012), so further investigation is necessary to determine what cellular processes are mediated by 5-HT_{1A} receptor activity that could produce effects large enough to be detectable by structural MRI.

We did not perform correction for partial volume effects (PVC) of the PET data as was done in Kraus et al. (Kraus et al. 2012). We think this was reasonable in this case, because our group of subjects was relatively young and no atrophy was anticipated; others have used a similar approach without PVC in similar investigations (Woodward et al. 2009).

For voxel-level analyses, we elected to use different smoothing kernels for each modality. As done by Kraus et al. (Kraus et al. 2012), an 8 mm kernel was used for spatially smoothing the VBM images, a default value typically used for analyses of VBM images with SPM. Kraus et al. did not specify whether a spatial smoothing was applied to the PET images, or which smoothing kernel was used. We applied spatial smoothing with a kernel of 4 mm to our [^{11}C] WAY100635 BP_F images to minimize spillover from the raphe nuclei region into neighboring structures. Using different kernel values for the spatial smoothing across modalities could have had an effect on the analysis; however, a comprehensive evaluation of the effects of varying smoothing kernels was outside the scope of the current investigation.

Both time of day and time of year may have an effect on 5-HT_{1A} receptor expression (Matheson et al. 2015). We did not standardize time of day or season for the PET imaging with [^{11}C]WAY100635. As the number of days into the year did not vary between MDD and control groups (see Table 1), this should not have had an effect on our group contrasts. The MDD group was scanned later in the day than the HC group (Table 1). The difference in time of scan between group means was only one hour, which we do not expect to influence our findings.

The MDD group had almost 2 years fewer of lifetime education, and years of education were positively associated to ROI-level GMV values only in the TEM among the MDD patients. However, repeating our ROI-level analysis adding number of years of education as a covariate did not change our findings.

We cannot exclude effects on [^{11}C]WAY100635 f_P of short acting benzodiazepines, whose use was allowed up to 24 h prior to PET scan for distressing anxiety or insomnia. However, these drugs have no meaningful affinity for the 5-HT_{1A} receptor (Braestrup and Squires 1978; Dompert et al. 1985).

Conclusions

We have replicated another group (Kraus et al. 2012) finding that, in the adult normative brain in vivo, postsynaptic 5-HT_{1A} receptor binding is positively correlated to GMV across most brain regions. We found no confirmation of such positive overall correlation in the adult brain in MDD. In contrast to previous finding (Kraus et al. 2012), we found in both groups a trend toward an inverse correlation between raphe 5-HT_{1A} autoreceptor binding and GMV in the anterior cingulate cortex, and a statistically significant positive correlation between raphe 5-HT_{1A} autoreceptor binding and cortical GMV in the temporal lobe in the MDD group. Divergent regional relationships between autoreceptor binding and terminal field GMV may be driven by differences in activity of serotonergic neurons within specific raphe nuclei subfields with differing projection patterns, or by differences in postsynaptic signal transduction in the terminal field.

Although we still cannot pinpoint the exact neuroplastic cellular processes that are mediated by 5-HT and the 5-HT_{1A} receptor, these results may provide new insights towards a more comprehensive understanding of the mechanisms behind the GMV alterations observed in MDD, indicate a target for antidepressant treatment, and suggest the need for longitudinal treatment studies to examine dependence of changes in GMV on 5-HT_{1A} binding changes.

References

Akimova E, Lanzenberger R, Kasper S (2009) The serotonin-1A receptor in anxiety disorders. Biol Psychiatry 66:627–635. 10.1016/j.biopsych.2009.03.012 [PubMed: 19423077]

Ashburner J (2007) A fast diffeomorphic image registration algorithm. NeuroImage. 38:95–113 10.1016/j.neuroimage.2007.07.007 [PubMed: 17761438]

Azmitia EC (2001) Modern views on an ancient chemical: serotonin effects on cell proliferation, maturation, and apoptosis. Brain Res Bull 56:413–424 [PubMed: 11750787]

Beck AT, Ward CH, Mendelson M, Mock J, Erbaugh J (1961) An inventory for measuring depression. Arch Gen Psychiatry 4:561–571 [PubMed: 13688369]

Benninghoff J et al. (2010) Serotonin depletion hampers survival and proliferation in neurospheres derived from adult neural stem cells. Neuropsychopharmacol 35:893–903. 10.1038/npp.2009.181

Borroto-Escuela DO et al. (2015a) Evidence for the existence of FGFR1–5-HT1A heteroreceptor complexes in the midbrain raphe 5-HT system biochem. Biophys Res Commun 456:489–493. 10.1016/j.bbrc.2014.11.112

Borroto-Escuela DO et al. (2015b) Enhancement of the FGFR1 signaling in the FGFR1–5-HT1A heteroreceptor complex in midbrain raphe 5-HT neuron systems. Relevance for neuroplasticity depression. Biochem Biophys Res Commun 463:180–186. 10.1016/j.bbrc.2015.04.133 [PubMed: 25957476]

Borroto-Escuela DO, Tarakanov AO, Fuxe K (2016) FGFR1–5-HT1A heteroreceptor complexes: implications for understanding and treating major. Depression Trends Neurosci 39:5–15. 10.1016/j.tins.2015.11.003 [PubMed: 26687454]

Braestrup C, Squires RF (1978) Pharmacological characterization of benzodiazepine receptors in the brain European. J Pharmacol 48:263–270

Casanova R et al. (2007) Biological parametric mapping: a statistical toolbox for multimodality brain. Image Anal Neuroimage 34:137–143. 10.1016/j.neuroimage.2006.09.011

Citri A, Malenka RC (2008) Synaptic plasticity: multiple forms, functions, and mechanisms. Neuropsychopharmacol 33:18–41. 10.1038/sj.npp.1301559

Dannlowski U et al. (2014) Serotonin transporter gene methylation is associated with hippocampal gray matter volume. Hum Brain Mapp 35:5356–5367. 10.1002/hbm.22555 [PubMed: 24862560]

Daubert EA, Condron BG (2010) Serotonin: a regulator of neuronal morphology and circuitry. Trends Neurosci 33:424–434. 10.1016/j.tins.2010.05.005 [PubMed: 20561690]

Dayer A (2014) Serotonin-related pathways and developmental plasticity: relevance for psychiatric disorders. Dialog Clin Neurosci 16:29–41

DeLorenzo CKA, Mikhno A, Gray N, Zanderigo F, Mann JJ, Parsey RV (2009) A new method for assessing PET-MRI coregistration In: Medical Imaging 2009: Image Processing; 2009, Lake Buena Vista SPIE, FL

Depping MS, Wolf ND, Vasic N, Sambataro F, Thomann PA, Christian Wolf R (2015) Specificity of abnormal brain volume in major depressive disorder: a comparison with borderline personality disorder. J Affective Disorders 174:650–657. 10.1016/j.jad.2014.11.059

Dompert WU, Glaser T, Traber J (1985) 3H-TVX Q 7821: identification of 5-HT1 binding sites as target for a novel putative anxiolytic Naunyn-Schmiedeberg's. Arch Pharmacol 328:467–470 [PubMed: 2859533]

Draganski B, Gaser C, Busch V, Schuierer G, Bogdahn U, May A (2004) Neuroplasticity: changes in grey matter induced. by training. Nature 427:311–312. 10.1038/427311a [PubMed: 14737157]

Drevets WC et al. (1999) PET imaging of serotonin 1A receptor binding in depression. Biol Psychiatry 46:1375–1387 [PubMed: 10578452]

Drevets WC, Thase ME, Moses-Kolko EL, Price J, Frank E, Kupfer DJ, Mathis C (2007) Serotonin-1A receptor imaging in recurrent depression: replication and literature review. Nuclear Med Biol 34:865–877. 10.1016/j.nucmedbio.2007.06.008

Duvernoy H (1991) The human brain: surface, three-dimensional sectional anatomy and MRI. New York

First MSR, Gibbon M, Williams J (1995) Structured clinical interview for DSM-IV axis I disorders (SCID-I/P, Version 2.0). Biometrics Research Dept., New York State Psychiatric Institute, New York

First MB, Spitzer RL, Gibbon M, Williams JB (2012) Structured clinical interview for DSM-IV® Axis I disorders (SCID-I), clinician version,. American Psychiatric Pub.

Gaspar P, Cases O, Maroteaux L (2003) The developmental role of serotonin: news from mouse molecular genetics. Nat Rev Neurosci 4:1002–1012. 10.1038/nrn1256 [PubMed: 14618156]

Geuze E, Vermetten E, Bremner JD (2005) MR-based in vivo hippocampal volumetrics: 1. Review of methodologies currently employed. Mol Psychiatry 10:147–159. 10.1038/sj.mp.4001580 [PubMed: 15340353]

Goodkind M et al. (2015) Identification of a common neurobiological substrate for mental illness. JAMA Psychiatry 72:305–315. 10.1001/jamapsychiatry.2014.2206 [PubMed: 25651064]

Gunn RN, Gunn SR, Turkheimer FE, Aston JA, Cunningham VJ (2002) Positron emission tomography compartmental models: a basis pursuit strategy for kinetic modeling. J Cereb Blood Flow Metabol 22:1425–1439. 10.1097/00004647-200212000-00003

Hamilton M (1960) A rating scale for depression. J Neurol Neurosurg Psychiatry 23:56–62 [PubMed: 14399272]

Hirvonen J et al. (2008) Decreased brain serotonin 5-HT1A receptor availability in medication-naive patients with major depressive disorder: an in-vivo imaging study using PET and [carbonyl-11C] WAY-100635. Int J Neuropsychopharmacol 11:465–476 [PubMed: 17971260]

Hsiung SC, Adlersberg M, Arango V, Mann JJ, Tamir H, Liu KP (2003) Attenuated 5-HT1A receptor signaling in brains of suicide victims: involvement of adenylyl cyclase, phosphatidylinositol 3-kinase, Akt and mitogen-activated protein kinase. J Neurochem 87:182–194 [PubMed: 12969265]

Innis RB et al. (2007) Consensus nomenclature for in vivo imaging of reversibly binding radioligands. J Cereb Blood Flow Metab 27:1533–1539. 10.1038/sj.jcbfm.9600493 [PubMed: 17519979]

Jasinska AJ, Lowry CA, Burmeister M (2012a) Corrigendum: serotonin transporter gene, stress, and raphe-raphe interactions: a molecular mechanism of depression. Trends Neurosci 35:454–455 [PubMed: 22919705]

Jasinska AJ, Lowry CA, Burmeister M (2012b) Serotonin transporter gene, stress and raphe-raphe interactions: a molecular mechanism of depression. Trends Neurosci 35:395–402. 10.1016/j.tins.2012.01.001 [PubMed: 22301434]

Kanai R, Rees G (2011) The structural basis of inter-individual differences in human behaviour and cognition. Nat Rev Neurosci 12:231–242. 10.1038/nrn3000 [PubMed: 21407245]

Kraus C et al. (2012) Serotonin-1A receptor binding is positively associated with gray matter volume—a multimodal neuroimaging study combining PET and structural. MRI NeuroImage 63:1091–1098. 10.1016/j.neuroimage.2012.07.035 [PubMed: 22836176]

Maldjian JA, Laurienti PJ, Kraft RA, Burdette JH (2003) An automated method for neuroanatomic and cytoarchitectonic atlas-based interrogation of fMRI data sets. NeuroImage 19:1233–1239 [PubMed: 12880848]

Malykhin NV, Coupland NJ (2015) Hippocampal neuroplasticity in major. depressive disorder. Neuroscience 309:200–213. 10.1016/j.neuroscience.2015.04.047 [PubMed: 25934030]

Matheson GJ et al. (2015) Diurnal and seasonal variation of the brain serotonin system in healthy male subjects. NeuroImage. 112:225–231 10.1016/j.neuroimage.2015.03.007 [PubMed: 25772667]

Maya Vetencourt JF et al. (2008) The antidepressant fluoxetine restores plasticity in the adult visual cortex. Science (New York, NY) 320:385–388. 10.1126/science.1150516

Meltzer CC et al. (2004) Serotonin 1A receptor binding and treatment response in late—life depression. Neuropsychopharmacology 29:2258–2265 [PubMed: 15483563]

Milak MS et al. (2010) In vivo quantification of human serotonin 1A receptor using 11C-CUMI-101, an agonist PET radiotracer. J Nuclear Med 51:1892–1900. 10.2967/jnumed.110.076257

Miller JM, Brennan KG, Ogden TR, Oquendo MA, Sullivan GM, Mann JJ, Parsey RV (2009) Elevated serotonin 1A binding in remitted major depressive disorder: evidence for a trait biological abnormality. Neuropsychopharmacology 34:2275–2284. 10.1038/npp.2009.54 [PubMed: 19458612]

Miller JM, Hesselgrave N, Ogden RT, Zanderigo F, Oquendo MA, Mann JJ, Parsey RV (2013) Brain serotonin 1A receptor binding as a predictor of treatment outcome in major depressive disorder. Biological psychiatry 74:760–767. 10.1016/j.biopsych.2013.03.021 [PubMed: 23664414]

Nautiyal KM, Hen R (2017) Serotonin receptors in depression: from A to B F1000Res 6:123 10.12688/f1000research.9736.1 [PubMed: 28232871]

Ogren SO et al. (2008) The role of 5-HT(1A) receptors in learning and memory. Behav Brain Res 195:54–77. 10.1016/j.bbr.2008.02.023 [PubMed: 18394726]

Parsey RV et al. (2000) Validation and reproducibility of measurement of 5-HT1A receptor parameters with [carbonyl-11C]WAY-100635 in humans: comparison of arterial and reference tisssue input functions. J Cereb Blood Flow Metab 20:1111–1133. 10.1097/00004647-200007000-00011 [PubMed: 10908045]

Parsey RV, Arango V, Olvet DM, Oquendo MA, Van Heertum RL, John Mann J (2005) Regional heterogeneity of 5-HT1A receptors in human cerebellum as assessed by positron emission

tomography. J Cereb Blood Flow Metab 25:785–793. 10.1038/sj.jcbfm.9600072 [PubMed: 15716853]

Parsey RV, Olvet DM, Oquendo MA, Huang YY, Ogden RT, Mann JJ (2006a) Higher 5-HT1A receptor binding potential during a major depressive episode predicts poor treatment response: preliminary data from a naturalistic study. Neuropsychopharmacol 31:1745–1749. 10.1038/sj.npp.1300992

Parsey RV et al. (2006b) Altered serotonin 1A binding in major depression: a [carbonyl-C-11]WAY100635 positron emission tomography study. Biol Psychiatry 59:106–113. 10.1016/j.biopsych.2005.06.016 [PubMed: 16154547]

Parsey RV et al. (2010) Higher serotonin 1A binding in a second major depression cohort: modeling and reference region considerations. Biol Psychiatry 68:170–178. 10.1016/j.biopsych.2010.03.023 [PubMed: 20497898]

Persico AM, Di Pino G, Levitt P (2006) Multiple receptors mediate the trophic effects of serotonin on ventroposterior thalamic neurons in vitro. Brain Res 1095:17–25. 10.1016/j.brainres.2006.04.006 [PubMed: 16701576]

Pike VW et al. (1996) Exquisite delineation of 5-HT1A receptors in human brain with PET and [carbonyl-11 C]WAY-100635. Eur J Pharmacol 301:R5–7 [PubMed: 8773468]

Pittenger C, Duman RS (2008) Stress, depression, and neuroplasticity: a convergence of mechanisms. Neuropsychopharmacol 33:88–109. 10.1038/sj.npp.1301574

Rabiner EA, Wilkins MR, Turkheimer F, Gunn RN, Udo de Haes J, de Vries M, Grasby PM (2002) 5-Hydroxytryptamine1A receptor occupancy by novel full antagonist 2-[4-[4-(7-chloro-2,3-dihydro-1,4-benzdioxyn-5-yl)-1-piperazinyl]butyl]-1,2-benzi sothiazol-3-(2H)-one-1,1-dioxide: a[11C][O-methyl-3H]-N-(2-(4-(2-methoxyphenyl)-1-piperazinyl)ethyl)-N-(2-pyridinyl) cyclohexanecarboxamide trihydrochloride (WAY-100635) positron emission tomography study in humans. J Pharmacol Exp Ther 301:1144–1150 [PubMed: 12023549]

Salvadore G et al. (2011) Prefrontal cortical abnormalities in currently depressed versus currently remitted patients with major depressive disorder. NeuroImage 54:2643–2651 10.1016/j.neuroimage.2010.11.011 [PubMed: 21073959]

Sargent PA et al. (2000) Brain serotonin1A receptor binding measured by positron emission tomography with [11C]WAY-100635: effects of depression and antidepressant treatment. Arch Gen Psychiatry 57:174–180 [PubMed: 10665620]

Savitz JB, Drevets WC (2009) Imaging phenotypes of major depressive disorder:. genetic correlates. Neuroscience 164:300–330. 10.1016/j.neuroscience.2009.03.082 [PubMed: 19358877]

Savitz J, Lucki I, Drevets WC (2009) 5-HT(1A) receptor function in major depressive. disorder. Prog Neurobiol 88:17–31. 10.1016/j.pneurobio.2009.01.009 [PubMed: 19428959]

Schmidt HD, Duman RS (2007) The role of neurotrophic factors in adult hippocampal neurogenesis, antidepressant treatments and animal models of depressive-like behavior. Behav Pharmacol 18:391–418. 10.1097/FBP.0b013e3282ee2aa8 [PubMed: 17762509]

Smith R, Chen K, Baxter L, Fort C, Lane RD (2013) Antidepressant effects of sertraline associated with volume increases in dorsolateral prefrontal cortex. J Affective Disord 146:414–419. 10.1016/j.jad.2012.07.029

Sullivan GM et al. (2015) Positron emission tomography quantification of serotonin(1A) receptor binding in suicide attempters with major depressive disorder. JAMA Psychiatry 72:169–178. 10.1001/jamapsychiatry.2014.2406 [PubMed: 25549105]

Talairach J, Tournoux P (1988) Co-planar stereotaxic atlas of the human brain: three-dimensional proportional system. Thieme Medical, New York

Tardito D, Perez J, Tiraboschi E, Musazzi L, Racagni G, Popoli M (2006) Signaling pathways regulating gene expression, neuroplasticity, and neurotrophic mechanisms in the action of antidepressants: a critical overview. Pharmacological reviews 58:115–134. 10.1124/pr.58.1.7 [PubMed: 16507885]

Tost H, Braus DF, Hakimi S, Ruf M, Vollmert C, Hohn F, Meyer-Lindenberg A (2010) Acute D2 receptor blockade induces rapid, reversible remodeling in human cortical-striatal circuits. Nat Neurosci 13:920–922. 10.1038/nn.2572 [PubMed: 20526332]

van Spronsen M, Hoogenraad CC (2010) Synapse pathology in psychiatric and neurologic disease. Curr Neurol Neurosci Rep 10:207–214. 10.1007/s11910-010-0104-8 [PubMed: 20425036]

van Tol MJ et al. (2010) Regional brain volume in depression and anxiety disorders. Arch Gen Psychiatry 67:1002–1011. 10.1001/archgenpsychiatry.2010.121 [PubMed: 20921116]

Woodward ND et al. (2009) Cerebral morphology and dopamine D2/D3 receptor distribution in humans: a combined [18F]fallypride and voxel-based morphometry study. NeuroImage. 46:31–38 10.1016/j.neuroimage.2009.01.049 [PubMed: 19457373]

Wright IC et al. (1995) A voxel-based method for the statistical analysis of gray and white matter density applied to schizophrenia. NeuroImage. 2:244–252 10.1006/nimg.1995.1032 [PubMed: 9343609]

Yan W, Wilson CC, Haring JH (1997) 5-HT1a receptors mediate the neurotrophic effect of serotonin on developing dentate granule cells. Brain Res Dev Brain Res 98:185–190 [PubMed: 9051259]

Zatorre RJ, Fields RD, Johansen-Berg H (2012) Plasticity in gray and white: neuroimaging changes in brain structure during learning. Nat Neurosci 15:528–536. 10.1038/nn.3045 [PubMed: 22426254]

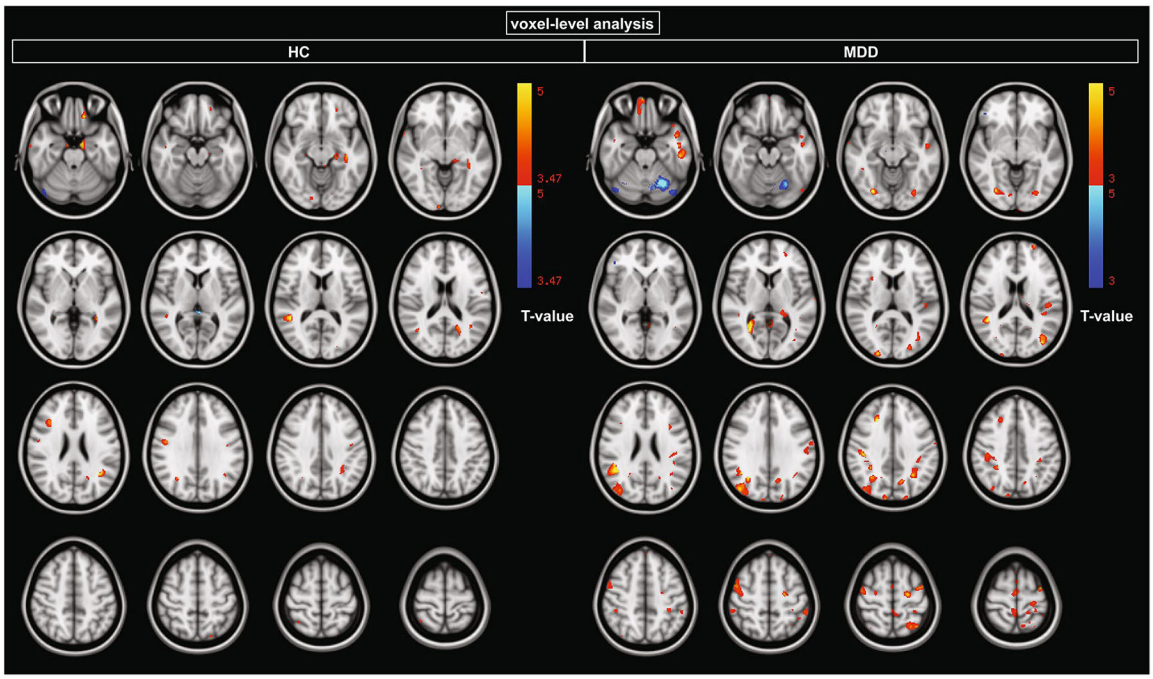

Fig. 1.

Clusters of statistically significant positive and negative correlations between 5-HT_{1A} $\log(BP_F)$, where log indicates the natural logarithm, and GMV using voxel-wise regression ($p < 0.05$ FDR-corrected)

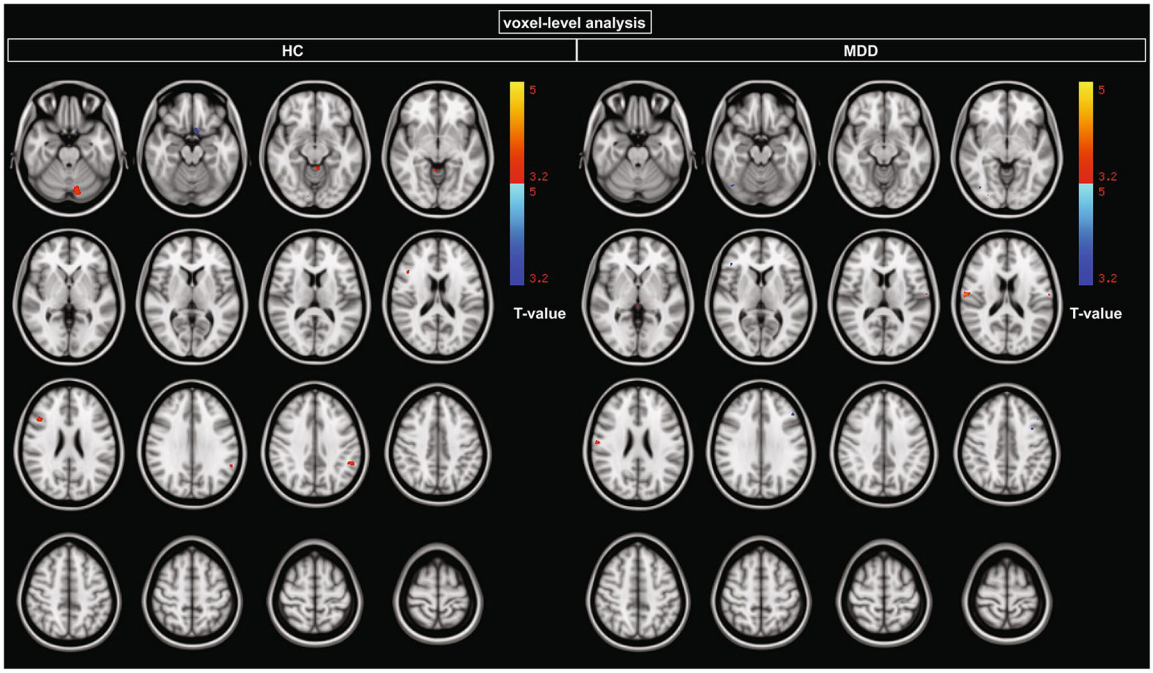

Fig. 2.

Relationship between GMV and raphe 5-HT_{1A} log(BP_F), where log indicates the natural logarithm, at an uncorrected threshold ($p < 0.001$). This exploratory threshold was applied when no results survived the threshold of $p < 0.05$, $k > 50$ corrected for multiple comparisons using FDR. At this uncorrected threshold, clusters larger than 215 voxels were deemed significant at $p < 0.05$ corrected

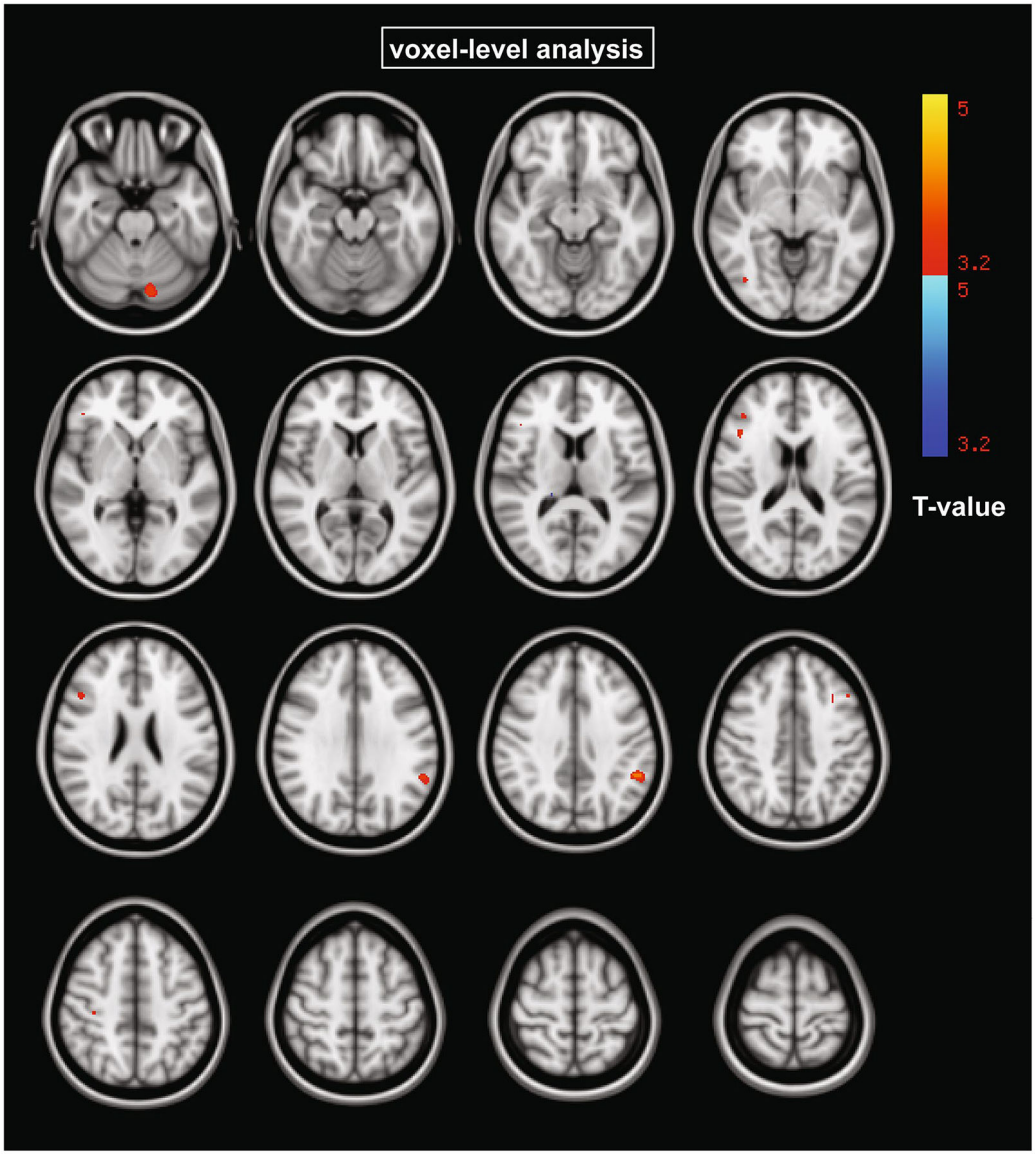

Fig. 3.

Clusters where correlations between raphe 5-HT_{1A} log(BP_F), where log indicates the natural logarithm, and each GMV voxel are moderated by diagnosis (cerebellum and supramarginal gyrus; $p < 0.001$ uncorrected). This exploratory threshold was applied when no results survived the threshold of $p < 0.05$, $k > 50$ corrected for multiple comparisons using FDR. At this uncorrected threshold, clusters larger than 215 voxels were deemed significant at $p < 0.05$ corrected

Table 1

Demographics, structural and radiochemical variables, and clinical information of the study samples

	HCs (*N* = 40)	**MDDs (*N* = 47)**	***p* value (HCs vs. MDDs two-tailed *t* test)**
Age (years)	38.0 ± 15.4	39.1 ± 12.1	0.70
HRSD (17 item)	0.8 ± 1.1	15.8 ± 7.1	< 0.001
BDI	1.5 ± 2.1	23.2 ± 12.6	< 0.001
Years of education	16.3 ± 2.7	14.5 ± 2.9	< 0.001
Age at onset	N/A	23.6 ± 12.5	
Number of previous depressive episodes	N/A	6.5 ± 15.8	
		Median: 3	
		Range: 0–99	
Length of current major depressive episode (weeks)	N/A	57.8 ± 92.5	
		Median: 32	
		Range: 3–584	
Weight (kg)	74.9 ± 19.7	74.8 ± 18.9	0.99
TGMV (cm^3)	643.2 ± 70.5	628.3 ± 62.6	0.30
Injected dose (MBq)	301.9 ± 131.8	293.2 ± 132.8	0.76
Specific activity (MBq/nmol)	54.4 ± 26.7	71.7 ± 42.0	0.03
Injected mass (μg)	3.1 ± 2.1	2.1 ± 1.2	0.01
Day of the year of PET scan	168 ± 111	205±110	0.13
Time of the day of PET scan (hours past midnight)	13.3 ± 1.2	14.3 ± 2.3	0.01
Categorical variables	***N* (%)**	***N* (%)**	***p* value (HCs vs. MDDs, Fisher's exact)**
Female	19 (48)	30 (64)	0.20
Prior exposure to anti-depressants	N/A	22 (47)	
Past substance abuse	N/A	13 (36)	
Comorbid anxiety disorder	N/A	21 (45)	
Comorbid dysthymia	N/A	6 (13)	
Race/ethnicity			
Asian	6 (15)	2 (4)	
African American	4 (10)	6 (13)	
Caucasian	22 (55)	27 (57)	

	HCs (N = 40)	MDDs (N = 47)	p value (HCs vs. MDDs two-tailed t test)
Hispanic	8 (20)	14 (30)	
> 1 Race	0 (0)	2 (4)	

HRSD: Hamilton rating scale for depression; BDI: Beck depression inventory

Table 2

Regions with statistically significant positive correlations between 5-HT_{1A} log(BP_F), where log indicates the natural logarithm, and GMV using voxel-wise regression in the HC group ($p < 0.05$ FDR-corrected, $k > 50$)

HC group, $p < 0.05$ FDR-corrected, $k > 50$					
Voxels	**Max**	**Max *X* (mm)**	**Max *Y* (mm)**	**Max *Z* (mm)**	**Cluster labels**
267	5.12	48	−44	11.5	37% Middle temporal gyrus, temporo-occipital part, 21% supramarginal gyrus, posterior division, 14% angular gyrus
258	4.64	−28	17	−39	71% Temporal pole
221	4.42	−34	−34	−8	5% Parahippocampal gyrus, posterior division, 2% temporal fusiform cortex, posterior division
219	5.03	−40	−55	24	35% Angular gyrus, 3% supramarginal gyrus, posterior division, 3% middle temporal gyrus, temporo-occipital part, 2% lateral occipital cortex, superior division
197	4.79	−54	−14	−39	18% Inferior temporal gyrus, posterior division, 3% inferior temporal gyrus, anterior division
195	4.91	−12	−8	−24	40% Parahippocampal gyrus, anterior division
160	4.19	−19	−26	−10	40% Parahippocampal gyrus, posterior division
148	4.46	−19	−60.5	19	39% Precuneous cortex, 32% supracalcarine cortex, 2% cuneal cortex, 2% intracalcarine cortex
145	4.57	37.5	21	24	19% Middle frontal gyrus, 14% inferior frontal gyrus, pars opercularis, 4% inferior frontal gyrus, pars triangularis, 2% precentral gyrus
135	4.68	49	−7	29	35% Precentral gyrus, 26% postcentral gyrus
119	4.64	−14	35	−24	38% Frontal orbital cortex, 16% frontal pole
99	4.88	−8	−43	−52	Brainstem
93	4.15	−30	−49	37	19% Superior parietal lobule, 5% supramarginal gyrus, posterior division, 2% lateral occipital cortex, superior division, 2% angular gyrus
82	4.13	−19	45.5	−16	65% Frontal pole
72	4.10	63	−10	−27.5	43% Middle temporal gyrus, posterior division, 12% middle temporal gyrus, anterior division, 7% inferior temporal gyrus, posterior division, 5% inferior temporal gyrus, anterior division
61	4.26	31	−62	32	27% Lateral occipital cortex, superior division, 1% angular gyrus
55	4.56	35	−54	63	43% Superior parietal lobule, 16% lateral occipital cortex, superior division, 1% supramarginal gyrus, posterior division
55	4.35	11	−98	−7.5	65% Occipital pole, 1% lingual gyrus

Table 3

Regions with statistically significant positive correlations between 5-HT_{1A} log(BP_F), where log indicates the natural logarithm, and GMV using voxel-wise regression in the MDD group ($p < 0.05$ FDR-corrected, $k > 50$)

MDD group, $p < 0.05$ FDR-corrected, $k > 50$					
Voxels	**Max**	**Max *X* (mm)**	**Max *Y* (mm)**	**Max *Z* (mm)**	**Cluster labels**
1985	4.65	−41	11	−35	49% Temporal pole, 1% inferior temporal gyrus, anterior division
1254	4.69	−52	−16	−28	44% Inferior temporal gyrus, posterior division, 4% temporal fusiform cortex, anterior division, 4% inferior temporal gyrus, anterior division, 1% temporal fusiform cortex, posterior division
1180	5.05	38	−74	31	53% Lateral occipital cortex, superior division
1171	4.47	42	11	−37	60% Temporal pole
958	4.73	−6	−13	70	34% Precentral gyrus, 24% juxtapositional lobule cortex (formerly supplementary motor cortex), 1% superior frontal gyrus
923	5.40	−22	−44	65	38% Postcentral gyrus, 22% superior parietal lobule, 1% supramarginal gyrus, anterior division
751	5.42	5	−41	71	36% Postcentral gyrus, 28% precuneous cortex
673	5.69	47	−49	24	63% Angular gyrus, 8% supramarginal gyrus, posterior division
595	4.11	47	−5	54	71% Precentral gyrus, 5% postcentral gyrus, 1% middle frontal gyrus
467	5.32	44	−31	42	31% Supramarginal gyrus, anterior division, 18% postcentral gyrus, 5% supramarginal gyrus, posterior division, 1% superior parietal lobule
405	4.65	−38	−74	16.5	28% Lateral occipital cortex, superior division, 17% lateral occipital cortex, inferior division
357	4.44	−28	−60	60	33% Lateral occipital cortex, superior division, 20% superior parietal lobule
345	5.63	27.5	−55	7	18% Precuneous cortex, 15% lingual gyrus, 5% intracalcarine cortex
337	3.79	−44	−29	18	67% Parietal operculum cortex, 5% planum temporale, 5% Heschl's gyrus (includes H1 and H2), 5% central opercular cortex, 1% superior temporal gyrus, posterior division
308	5.12	27	−76	−9	59% Occipital fusiform gyrus, 4% lingual gyrus, 3% lateral occipital cortex, inferior division
301	4.31	8	51	−24	52% Frontal pole, 20% frontal medial cortex
270	4.44	−33	−55	34	9% Lateral occipital cortex, superior division, 6% angular gyrus, 6% supramarginal gyrus, posterior division, 5% superior parietal lobule
228	4.64	−22	−13	57.5	15% Precentral gyrus, 12% superior frontal gyrus
225	3.84	−29	−78	−10	62% Occipital fusiform gyrus, 7% lateral occipital cortex, inferior division, 1% lingual gyrus
214	4.09	−12	−66	35	26% Precuneous cortex, 6% cuneal cortex, 1% lateral occipital cortex, superior division
210	5.03	−1.5	−53	5	3% Lingual gyrus, 2% precuneous cortex, 1% cingulate gyrus, posterior division, 1% intracalcarine cortex
204	4.95	−37.5	−5	62	42% Precentral gyrus, 18% middle frontal gyrus
189	4.92	24	26	38	23% Middle frontal gyrus, 9% superior frontal gyrus
161	3.44	−57	−17	32	55% Postcentral gyrus, 10% supramarginal gyrus, anterior division

MDD group, $p < 0.05$ FDR-corrected, $k > 50$					
Voxels	**Max**	**Max *X* (mm)**	**Max *Y* (mm)**	**Max *Z* (mm)**	**Cluster labels**
139	4.28	12	−89	36	53% Occipital pole, 17% lateral occipital cortex, superior division, 2% cuneal cortex
133	3.65	−53	−39.5	52	35% Supramarginal gyrus, anterior division, 33% supramarginal gyrus, posterior division, 3% superior parietal lobule, 1% angular gyrus, 1% postcentral gyrus
123	4.67	22	−96	13.5	70% Occipital pole
113	3.74	−21	−37.5	7	Posterior hippocampus
111	3.77	39.5	−15	−40.5	22% Temporal fusiform cortex, posterior division, 7% inferior temporal gyrus, posterior division, 2% inferior temporal gyrus, anterior division, 1% temporal fusiform cortex, anterior division
110	4.79	32	−45	39	24% Superior parietal lobule, 9% supramarginal gyrus, posterior division, 4% angular gyrus
105	3.77	−18	−89.5	33	41% Occipital pole, 18% lateral occipital cortex, superior division, 1% cuneal cortex
92	4.87	−41	−47	−41	Cerebellum
82	3.91	−25	−87	11.5	20% Lateral occipital cortex, superior division, 7% occipital pole, 6% lateral occipital cortex, inferior division
65	4.33	−25.5	60	19	82% Frontal pole
61	3.57	28	5	−40.5	41% Temporal pole, 35% temporal fusiform cortex, anterior division, 4% parahippocampal gyrus, anterior division, 1% temporal fusiform cortex, posterior division, 1% inferior temporal gyrus, anterior division

Table 4

Regions where correlations between voxel-wise 5-HT_{1A} log(BP_F), where log indicates the natural logarithm, and GMV are greater (HC > MDD) or smaller (HC < MDD) in the HC vs. MDD group, $p < 0.001$ uncorrected, $k > 10$)

Diagnosis by BP_F interaction, $p < 0.001$ uncorrected, $k > 10$					
Voxels	**Max**	**Max *X* (mm)**	**Max *Y* (mm)**	**Max *Z* (mm)**	**Cluster labels**
HC > MDD					
15	3.48	35	−41	−6	10% Lingual gyrus, 7% temporal occipital fusiform cortex, 1% parahippocampal gyrus, posterior division
13	3.35	−19	−75	−15	33% Occipital fusiform gyrus, 20% lingual gyrus
HC < MDD					
146	3.97	45	−9	57	52% Precentral gyrus, 13% postcentral gyrus
57	3.73	29	−58	5.5	12% Lingual gyrus, 7% intracalcarine cortex, 2% precuneous cortex
35	3.85	0	8	69	32% Juxtapositional lobule cortex (formerly supplementary motor cortex), 5% superior frontal gyrus
33	3.62	−9	−46	72	37% Postcentral gyrus, 13% superior parietal lobule, 12% precuneous cortex, 2% lateral occipital cortex, superior division, 1% precentral gyrus
19	3.63	−25	−43	72	31% Superior parietal lobule, 23% postcentral gyrus, 1% supramarginal gyrus, anterior division
15	3.34	−2	−9	73	18% Juxtapositional lobule cortex (formerly supplementary motor cortex), 8% precentral gyrus
13	3.90	−40	−50	−41	cerebellum
10	3.43	10	−41	78	62% Postcentral gyrus, 6% superior parietal lobule, 3% precuneous cortex, 2% precentral gyrus

This exploratory threshold was applied when no results survived the threshold of $p < 0.05$, $k > 50$ corrected for multiple comparisons using FDR. At this uncorrected threshold, clusters larger than 215 voxels were deemed significant at $p < 0.05$ corrected

Table 5

Regions with positive or negative correlations (direction indicated by sign of *T* value) between raphe 5-HT_{1A} log(BP_F), where log indicates the natural logarithm, and voxel-wise GMV in HC (top table), MDD (middle table), and moderated by diagnosis (bottom table) at $p < 0.001$ uncorrected, $k > 10$)

Region	*x*	*y*	*z*	Voxels	*T* value
HC group, *p* value < 0.001 uncorrected, *k* > 10					
Cerebellum	−13	−76	−29	547	4
25% Inferior frontal gyrus, pars opercularis, 6% inferior frontal gyrus, pars triangularis, 5% middle frontal gyrus, 4% precentral gyrus	44	20	22	133	3.98
38% Supramarginal gyrus, posterior division, 8% angular gyrus, 3% parietal operculum cortex, 2% supramarginal gyrus, anterior division, 1% planum temporale	−54	−45	34	103	3.88
Cerebellum	−2	−45	−10	88	3.67
38% Lingual gyrus, 22% occipital fusiform gyrus, 8% occipital pole, 1% lateral occipital cortex, inferior division	10	−85.5	−9	39	3.61
63% subcallosal cortex, 4% frontal orbital cortex	−8	12	−19.5	371	−3.94
48% Precuneous cortex, 30% cingulate gyrus, posterior division	−7	−54	32	228	−2.75
34% Lateral occipital cortex, superior division, 8% precuneous cortex, 2% cuneal cortex	18	−66	48	37	−2.74
26% Temporal pole, 25% parahippocampal gyrus, anterior division, 5% temporal fusiform cortex, anterior division, 1% inferior temporal gyrus, anterior division	19	5	−40	33	−2.69
MDD group, *p* value < 0.001 uncorrected, *k* > 10					
28% Central opercular cortex, 27% postcentral gyrus, 4% supramarginal gyrus, anterior division, 3% parietal operculum cortex, 2% precentral gyrus, 1% planum temporale	61	−12.5	19	168	4.2
48% Postcentral gyrus, 25% central opercular cortex, 2% parietal operculum cortex, 2% precentral gyrus, 1% planum temporale	−62	−13	16	24	3.44
55% Lateral occipital cortex, inferior division, 14% occipital fusiform gyrus	43	−71	−14	420	−3.6
47% Middle frontal gyrus, 3% inferior frontal gyrus, pars triangularis, 1% inferior frontal gyrus, pars opercularis	−45	24.5	33	418	−3.55
17% Inferior frontal gyrus, pars triangularis, 10% frontal pole, 3% middle frontal gyrus	44	33	10	413	−3.55
25% Middle frontal gyrus, 14% precentral gyrus	−37	5	44	219	−3.26
23% Middle temporal gyrus, posterior division, 20% middle temporal gyrus, temporo-occipital part, 3% inferior temporal gyrus, temporo-occipital part, 3% inferior temporal gyrus, posterior division	60	−38	−9	115	−3.28
28% Planum temporale, 13% superior temporal gyrus, posterior division, 8% supramarginal gyrus, posterior division, 4% parietal operculum cortex, 1% angular gyrus, 1% middle temporal gyrus, posterior division	60	−33	17	109	−3.08
52% Middle frontal gyrus	44.5	25	38	105	−2.81
31% Supramarginal gyrus, posterior division, 11% angular gyrus, 3% parietal operculum cortex	−50	−48	36.5	75	−2.85
27% Angular gyrus, 17% lateral occipital cortex, superior division, 5% supramarginal gyrus, posterior division, 5% superior parietal lobule	−37	−57	39	70	−3.08
40% Postcentral gyrus, 20% precentral gyrus	37	−21	46	69	−2.7
41% Postcentral gyrus, 25% precentral gyrus	36	−24	60	62	−2.56

Region	*x*	*y*	*z*	Voxels	*T* value
8% Frontal pole, 2% inferior frontal gyrus, pars triangularis, 1% frontal orbital cortex	−37	41	2	57	−2.89
31% Cingulate gyrus, anterior division, 29% paracingulate gyrus	−11	34.5	21	40	−2.78
47% Middle frontal gyrus	32	24	43	30	−2.86
42% Precuneous cortex, 18% cuneal cortex, 11% supracalcarine cortex, 1% intracalcarine cortex	−16.5	−67	24	26	−2.53
34% Middle temporal gyrus, temporo-occipital part, 6% inferior temporal gyrus, temporo-occipital part, 2% middle temporal gyrus, posterior division, 1% inferior temporal gyrus, posterior division	−54	−48	−6	18	−2.67
52% Temporal occipital fusiform cortex, 16% occipital fusiform gyrus, 1% inferior temporal gyrus, temporo-occipital part	36	−58	−14	15	−2.56
Diagnosis by BP_F, *p* value < 0.001 uncorrected, k > 10					
HC > MDD					
Cerebellum	−11	−77	−27.5	393	4.07
38% Supramarginal gyrus, posterior division, 10% angular gyrus, 3% parietal operculum cortex, 1% planum temporale	−53	−47	34	241	4.42
22% Inferior frontal gyrus, pars opercularis, 5% inferior frontal gyrus, pars triangularis, 3% precentral gyrus, 1% middle frontal gyrus	45	20	22	95	3.9
23% Middle frontal gyrus, 23% frontal pole, 19% inferior frontal gyrus, pars triangularis	41	35	16	36	3.49
51% Middle frontal gyrus, 2% inferior frontal gyrus, pars opercularis	−46	19	39	34	3.71
20% Middle frontal gyrus, 2% superior frontal gyrus	−32	18	43	15	3.28
23% Frontal pole, 21% inferior frontal gyrus, pars triangularis, 6% frontal orbital cortex, 1% frontal operculum cortex	44	36	2	12	3.45
53% Lateral occipital cortex, inferior division, 5% occipital fusiform gyrus	40.5	−70	−5.45	11	3.39

This exploratory threshold was applied when no results survived the threshold of $p < 0.05$, $k > 50$ corrected for multiple comparisons using FDR. At this uncorrected threshold, clusters larger than 215 voxels were deemed significant at $p < 0.05$ corrected